NASA Technical Paper 1639

# Aliased Noise in Radiometric Measurements

Friedrich O. Huck, Stephen K. Park,
Nesim Halyo, and Steven T. Stallman

MAY 1980

NASA

NASA Technical Paper 1639

# Aliased Noise in Radiometric Measurements

Friedrich O. Huck and Stephen K. Park
*Langley Research Center*
*Hampton, Virginia*

Nesim Halyo and Steven T. Stallman
*Information and Control Systems*
*Hampton, Virginia*

National Aeronautics
and Space Administration

**Scientific and Technical
Information Office**

1980

## SUMMARY

The reconstructed magnitude of radiance fluctuations (or fields) from discrete radiometric measurements is subject to errors caused by the aliased noise generated when the radiometer undersamples the spatial detail of these fluctuations. Quantitative results indicate that aliased noise can be a large source of error in the reconstruction process when the sampling intervals equal the instantaneous field of view (IFOV) of the radiometer (i.e., for contiguous coverage). This noise can be reduced about 2 orders of magnitude by shaping the effective IFOV (formed by the photosensor aperture and signal electronics) of a scanning radiometer and modestly decreasing the sampling intervals relative to the IFOV (to provide some overlap between successive measurements). In contrast, spatially smoothed (i.e., low-pass filtered) reconstructions of the discrete measurements provide only a relatively modest decrease in this noise at the cost of spatial resolution.

## INTRODUCTION

The reconstruction of spatial radiance fluctuations (or fields) is subject to errors caused by the aliased noise that is generated if spatial details have been undersampled. The resultant degradation of image quality obtained with line-scan devices (e.g., television cameras and optical-mechanical scanners) has received considerable attention in the literature (refs. 1 to 9). These investigations have emphasized spatial resolution: the reproduction, detection, recognition, and identification of detail. The accurate reconstruction of the radiance magnitude, or of spatial averages of the radiance magnitude, has been of little concern. The degradation of radiometric accuracy due to aliased noise has (to the authors' knowledge) never been quantitatively determined, except for a few illustrative examples (refs. 6 and 10).

This investigation formulates and computes the magnitude of the aliased noise that degrades the accuracy of continuous reconstructions of discrete radiometric measurements. It provides evaluations, in particular, of the magnitude of aliased noise as a function of the spatial (or angular) response and sampling interval of the radiometer and of the resolution of the reconstructed measurements. To produce generally useful results, a Wiener spectrum that is approximately representative of a wide range of scenes is used to characterize the (random) radiance fluctuations. This spectrum can be derived if the radiance fluctuations are assumed to be a random set of two-dimensional pulses whose width and magnitude obey the Poisson and the Gaussian probability density function, respectively.

## SYMBOLS

| | |
|---|---|
| a,b | photosensor aperture shape functions, m (see fig. 3) |

| | |
|---|---|
| $g(x,y)$ | spatial function |
| $\hat{g}(\upsilon,\omega)$ | spatial frequency spectrum of $g(x,y)$, $m^2$ |
| $J_1$ | first-order Bessel function |
| $L(x,y)$ | radiance fluctuations, $Wm^{-2}$ |
| $\hat{L}(\upsilon,\omega)$ | frequency spectrum of radiance fluctuations, W |
| $m(x,y)$ | continuous signal, W |
| $\bar{m}(x,y)$ | continuous signal of smoothed measurements, W |
| $m(x,y;X,Y)$ | discrete measurements, W (see fig. 1) |
| $\hat{m}(\upsilon,\omega;X,Y)$ | frequency spectrum of measurements, $Wm^2$ (see fig. 5) |
| $m,n$ | measurement count along x- and y-axis, respectively |
| $M,N$ | constants that determine rectangular dimensions of resel |
| $r$ | $= \lfloor (x_1 - x_2)^2 + (y_1 - y_2)^2 \rfloor^{1/2}$ |
| $R$ | resolution cell (resel), $m^2$ |
| $x,y$ | measurement coordinates, m (see fig. 1) |
| $X,Y$ | sampling intervals, m (see fig. 1) |
| $\gamma$ | equivalent instantaneous field of view (IFOV), m (see fig. 3) |
| $\delta(x)$ | unit impulse function, $m^{-1}$ |
| $\delta(x,y)$ | two-dimensional unit impulse function, $m^{-2}$ |
| $\theta$ | angle in the xy-plane, deg |
| $\mu$ | (expected) mean value, $Wm^{-2}$ |
| $\upsilon,\omega$ | spatial frequency along x- and y-axis, respectively, $m^{-1}$ (cycles/m) |
| $\rho$ | $= \lceil \upsilon^2 + \omega^2 \rceil^{1/2}$ |
| $\sigma$ | standard deviation, $Wm^{-2}$ |
| $\bar{\sigma}$ | standard deviation of smoothed measurements |
| $\tau(x,y)$ | spatial response (or point-spread function) |

$\hat{\tau}(\upsilon,\omega)$ spatial frequency response (or modulation transfer function (MTF))

$\Phi(\cdot)$ autocovariance, $W^2m^{-4}$

$\hat{\Phi}(\cdot)$ Wiener (or power density) spectrum, $W^2m^{-2}$ ($W^2m^{-4}/cycles^2m^{-2}$)

$\Pi(\cdot)$ rectangle function

$\amalg(\cdot)$ sampling or comb function

$*$ convolution

Subscripts:

a aliased noise, or sideband component generated by sampling

e electronic filter

$\ell$ lens

L radiance fluctuations

m measurement

p photosensor aperture

r interval between radiance fluctuations

R continuous signal reconstructed from discrete measurements

s sufficiently sampled signal components

## DEFINITIONS, ASSUMPTIONS, AND FORMULATIONS

### Measurement Process

This paper analyzes the linear, space-invariant measurement process shown in figure 1 that transfers the (continuous) radiance fluctuations $L(x,y)$ into a (discrete) signal $m(x,y;X,Y)$ as defined by the equations

$$m(x,y) = L(x,y) * \tau(x,y) \tag{1a}$$

$$m(x,y;X,Y) = m(x,y)\ \amalg\left(\frac{x}{X},\frac{y}{Y}\right) = [L(x,y) * \tau(x,y)]\ \amalg\left(\frac{x}{X},\frac{y}{Y}\right) \tag{1b}$$

where the symbol * denotes convolution; $\tau(x,y)$, the spatial response (or point-spread function) of the radiometer; and $\text{Ш}\left(\frac{x}{X},\frac{y}{Y}\right)$, the sampling (ref. 11) or comb (ref. 12) function given by

$$\text{Ш}\left(\frac{x}{X},\frac{y}{Y}\right) = \sum_{m=-\infty}^{\infty}\sum_{n=-\infty}^{\infty} \delta\left(\frac{x}{X} - m,\ \frac{y}{Y} - n\right) = XY \sum_{m=-\infty}^{\infty}\sum_{n=-\infty}^{\infty} \delta(x - Xm,\ y - Yn)$$

The discrete measurements $m(x,y;X,Y)$ are an infinite array of unit impulse functions on the rectangular lattice with spacing $X$ and $Y$ in the x- and y-directions, respectively. Rectangular (Cartesian) coordinates $(x,y)$ in the object or photosensor aperture plane are used as the reference for the measurement coordinates.

Salient properties of the measurements $m(x,y;X,Y)$ defined by equation (1b) are often more conveniently evaluated in the frequency domain than in the spatial domain. The functions $\hat{g}(\upsilon,\omega)$ and $g(x,y)$ are denoted as the Fourier transform pairs given by

$$\hat{g}(\upsilon,\omega) = \int_{-\infty}^{\infty}\int g(x,y)e^{-i2\pi(\upsilon x+\omega y)}\,dx\,dy \tag{2a}$$

$$g(x,y) = \int_{-\infty}^{\infty}\int \hat{g}(\upsilon,\omega)e^{i2\pi(x\upsilon+y\omega)}\,d\upsilon\,d\omega \tag{2b}$$

The Fourier transform of equation (1b) yields

$$\hat{m}(\upsilon,\omega;X,Y) = \hat{L}(\upsilon,\omega)\ \hat{\tau}(\upsilon,\omega) * XY\ \text{Ш}(X\upsilon,Y\omega) \tag{3a}$$

where

$$XY\ \text{Ш}(X\upsilon,Y\omega) = XY \sum_{m=-\infty}^{\infty}\sum_{n=-\infty}^{\infty} \delta(X\upsilon - m,\ Y\omega - n) = \sum_{m=-\infty}^{\infty}\sum_{n=-\infty}^{\infty} \delta\left(\upsilon - \frac{m}{X},\ \omega - \frac{n}{Y}\right)$$

Equation (3a) can be equivalently written as

$$\hat{m}(\upsilon,\omega;X,Y) = \sum_{m=-\infty}^{\infty} \sum_{n=-\infty}^{\infty} \hat{L}\left(\upsilon - \frac{m}{X}, \omega - \frac{n}{Y}\right) \cdot \hat{\tau}\left(\upsilon - \frac{m}{X}, \omega - \frac{n}{Y}\right) \tag{3b}$$

## Radiance Fluctuation

The magnitude of aliased noise in continuous reconstructions of discrete radiometric measurements depends on the properties of the radiance fluctuations $L(x,y)$ as well as on the spatial response $\tau(x,y)$ and the sampling intervals $(X,Y)$. In this paper a random radiance fluctuation that is both homogeneous and isotropic (ref. 13) is assumed, so that the variance of $L(x,y)$ is independent of $(x,y)$, and the autocovariance (and autocorrelation) is a function only of the relative distance

$$r = [(x_1 - x_2)^2 + (y_1 - y_2)^2]^{1/2} \tag{4}$$

between points $(x_1,y_1)$ and $(x_2,y_2)$. It follows that the assumed distribution of $L(x,y)$ is circularly symmetric.

Furthermore, the autocovariance of $L(x,y)$ is assumed to be

$$\Phi_L(r) = \sigma_L^2 \, e^{-r/\mu_r} \tag{5}$$

Then, the associated Wiener (or power density) spectrum, which is the circularly symmetric Fourier transform (i.e., the Hankel transform) of $\Phi_L(r)$, is

$$\hat{\Phi}_L(\upsilon,\omega) = \hat{\Phi}_L(\rho) = \frac{2\pi\mu_r^2\sigma_L^2}{[1 + (2\pi\mu_r\rho)^2]^{3/2}} \tag{6}$$

where $\rho^2 = \upsilon^2 + \omega^2$. (See fig. 2.) Equations (5) and (6) can be derived by assuming that $L(x,y)$ is a set of pulses whose random location in the xy-plane obeys the Poisson probability density function with the (expected) mean width $\mu_r$ and whose random magnitude obeys the Gaussian probability density function with the (expected) mean and variance $\mu_L$ and $\sigma_L^2$, respectively. (For derivations and further details, see refs. 14 and 15; for a detailed one-dimensional analysis, see ref. 16.) The variance $\sigma_L^2$ and the Wiener spectrum $\hat{\Phi}_L(\upsilon,\omega)$ are related by

$$\sigma_L^2 = \Phi_L(0) = \int_{-\infty}^{\infty}\int \Phi_L(\upsilon,\omega)\ d\upsilon\ d\omega = 2\pi \int_0^{\infty} \rho\hat{\Phi}_L(\rho)\ d\rho \tag{7}$$

That is, $\sigma_L^2$ is the value of the integrated Wiener spectrum.

## Radiometer Response

The spatial frequency response (or modulation transfer function (MTF)) $\hat{\tau}(\upsilon,\omega)$ of a radiometer can generally be characterized as

$$\hat{\tau}(\upsilon,\omega) = \hat{\tau}_\ell(\upsilon,\omega)\ \hat{\tau}_p(\upsilon,\omega)\ \hat{\tau}_e(\omega) \tag{8}$$

where $\hat{\tau}_\ell(\upsilon,\omega)$, $\hat{\tau}_p(\upsilon,\omega)$, and $\hat{\tau}_e(\omega)$, respectively, are the frequency response of the objective lens, photosensor aperture, and electronic filter; $\omega$ is the spatial frequency component in the line-scan direction. The photosensor aperture and its distance from the lens define the IFOV of the radiometer. The lens aperture and IFOV govern the total amount of radiance focused onto the photosensor aperture; however, unlike for high-resolution imaging devices, the (diffraction-limited) spatial frequency response of the lens usually does not significantly affect the frequency response of relatively low-resolution radiometers and is neglected in this paper.

Figure 3 illustrates salient characteristics of three photosensor aperture shapes. These apertures have equivalent areas, namely $\pi\gamma^2/4$. Thus for each aperture,

$$\int_{-\infty}^{\infty}\int_{-\infty}^{\infty} \tau_p(x,y)\ dx\ dy = \hat{\tau}_p(0,0) = 1$$

and

$$\tau_p(x,y) = \begin{cases} \dfrac{4}{\pi}\gamma^2 & ((x,y)\ \text{aperture area}) \\ 0 & (\text{elsewhere}) \end{cases}$$

It is convenient to regard the diameter $\gamma$ of the circular aperture as the equivalent IFOV of the three apertures. The spatial frequency response $\hat{\tau}_p(\upsilon,\omega)$ of the aperture shapes illustrated in figure 3 is given by the

following expressions, in which the shape parameters a and b are the x- and y-axis intercepts, respectively, of the apertures, and sinc x = sin $(\pi x)/\pi x$:

(a) Circular -

$$\hat{\tau}_p(\upsilon,\omega) = \hat{\tau}_p(\rho) = \frac{J_1(2\pi a\rho)}{\pi a\rho} \tag{9}$$

where $a = \frac{\gamma}{2}$

(b) Cosine -

$$\hat{\tau}_p(\upsilon,\omega) = \frac{4}{\pi}\int_0^{\pi/2} \cos(a\upsilon\theta)\ \text{sinc}(2b\omega\cos^2\theta)\cos^2\theta\, d\theta \tag{10}$$

where $a = \frac{\pi}{4}\gamma \qquad b = \frac{\gamma}{2}$

(c) Diamond -

$$\hat{\tau}_p(\upsilon,\omega) = \text{sinc}(a\upsilon + b\omega)\ \text{sinc}(a\upsilon - b\omega) \tag{11}$$

where $a = \frac{\pi}{4}\gamma \qquad b = \frac{\gamma}{2}$

The effect of various photosensor aperture shapes and profiles on the image quality obtained with line-scan devices has been investigated most notably by Mertz and Gray (ref. 1) for facsimile scanners and by Schade (ref. 2) for television cameras. One of their conclusions was that all reasonable profiles and shapes of equivalent size result in about equal blurring, but that some of the profiles and shapes tend to suppress aliasing better than others. Katzberg et al. (ref. 6) demonstrated that the cosine and diamond shapes are both superior to the circular shape in suppressing aliasing.

The cosine and diamond apertures are shaped to suppress side lobes along the $\upsilon$-spatial frequency axis normal to the line-scan direction. The exact aperture shape along the line-scan direction is less important in continuously

scanning devices, since the effective $\omega$-spatial frequency response can be reshaped by an electronic low-pass filter. The function given by

$$\hat{\tau}_e(\omega) = \begin{cases} 1 - (\gamma\omega)^4 & (|\omega| < 1/\gamma) \\ 0 & (|\omega| > 1/\gamma) \end{cases} \tag{12}$$

and shown in figure 4 was chosen to represent the spatial frequency response of an electronic filter. The cutoff frequency $1/\gamma$ provides a useful spatial frequency passband for the radiometer that is approximately circularly symmetric. In practice, it might often be preferable to eliminate aliasing along the line-scan direction by selecting a cutoff frequency equal to $1/2Y$.

## Signal and Aliased Noise

The discrete measurements $m(x,y;X,Y)$ defined by equation (1b) have a mean value $\mu_L$ and a Wiener spectrum $\hat{\Phi}_m(\upsilon,\omega;X,Y)$ given by

$$\hat{\Phi}_m(\upsilon,\omega;X,Y) = \hat{\Phi}_s(\upsilon,\omega) + \hat{\Phi}_a(\upsilon,\omega;X,Y) \tag{13}$$

The term $\hat{\Phi}_s(\upsilon,\omega)$ represents the (desired) fundamental signal component centered at the location $(\upsilon,\omega) = (0,0)$ and is given by

$$\hat{\Phi}_s(\upsilon,\omega) = \hat{\Phi}_L(\upsilon,\omega) \left|\hat{\tau}(\upsilon,\omega)\right|^2 \tag{14}$$

The term $\hat{\Phi}_a(\upsilon,\omega;X,Y)$ represents the (undesired) sampling sideband components centered at the locations $(\upsilon,\omega) = \left(\frac{m}{X},\frac{n}{Y}\right)$, $(m,n) \neq (0,0)$, and is given by

$$\hat{\Phi}_a(\upsilon,\omega;X,Y) = \sum_{m=-\infty}^{\infty} \sum_{n=-\infty}^{\infty} \hat{\Phi}_s\left(\upsilon - \frac{m}{X},\ \omega - \frac{n}{Y}\right) \tag{15}$$

$$(m,n) \neq (0,0)$$

The development of equation (15) from equations (1) is standard. (See for example, refs. 10 and 13.)

The frequency passband of the sampling lattice with spacing (X,Y), or briefly the sampling passband, is given by the rectangle function (ref. 11)

$$\Pi(X\upsilon,Y\omega) = \begin{cases} 1 & \left(|\upsilon| < \frac{1}{2X},\ |\omega| < \frac{1}{2Y}\right) \\ 0 & \text{(elsewhere)} \end{cases} \tag{16}$$

The variance $\sigma_s^2$ of the fundamental signal component within the sampling passband is

$$\sigma_s^2 = \int_{-\infty}^{\infty}\int_{-\infty}^{\infty} \hat{\Phi}_s(\upsilon,\omega)\ \Pi(X\upsilon,Y\omega)\ d\upsilon\ d\omega = \int_{-1/2X}^{1/2X}\int_{-1/2Y}^{1/2Y} \hat{\Phi}_s(\upsilon,\omega)\ d\upsilon\ d\omega \tag{17}$$

and the variance $\sigma_a^2$ of the sampling sideband components within the sampling passband is

$$\sigma_a^2 = \int_{-\infty}^{\infty}\int_{-\infty}^{\infty} \hat{\Phi}_a(\upsilon,\omega;X,Y)\ \Pi(X\upsilon,Y\omega)\ d\upsilon\ d\omega = \int_{-1/2X}^{1/2X}\int_{-1/2Y}^{1/2Y} \hat{\Phi}_a(\upsilon,\omega;X,Y)\ d\upsilon\ d\omega \tag{18}$$

If the Wiener spectrum $\hat{\Phi}_L(\upsilon,\omega)$ of the radiance fluctuations or the spatial frequency response $\hat{\tau}(\upsilon,\omega)$ of the radiometer is contained within the sampling passband (i.e., if $\hat{\Phi}_s(\upsilon,\omega) = 0$ outside the sampling passband), then $\sigma_a^2 = 0$, and the signal is said to be sufficiently sampled. Otherwise, the signal is insufficiently sampled, and displaced frequency components from the sidebands fall into the sampling passband, as illustrated in figure 5. These displaced frequency components cannot be distinguished in practice from the desired signal - they tend to behave, and are treated here, as additive noise. This treatment follows Blackman and Tukey (ref. 17), who define aliased noise as those components of the signal that are contained in the signal only when insufficient sampling occurs. Insufficient sampling occurs frequently in practice because the spatial frequency response $\hat{\tau}(\upsilon,\omega)$ of optical systems tends to decrease very gradually and to oscillate around zero.

The function $m_R(x,y)$ is denoted as a continuous reconstruction of the discrete measurements $m(x,y;X,Y)$; the spatial resolution of this reconstruction is defined as the resolution cell (resel) R. If the rectangle function $\Pi(X\upsilon,Y\omega)$ given by equation (16) is the reconstruction filter, then $m_R(x,y)$ is the inverse Fourier transform of $\hat{m}(\upsilon,\omega;X,Y)\ \Pi(X\upsilon,Y\omega)$; that is,

$$m_R(x,y) = \sum_{m=-\infty}^{\infty} \sum_{n=-\infty}^{\infty} m(mX,nY)\ \text{sinc}\left(\frac{x - mX}{X}\right) \text{sinc}\left(\frac{y - nY}{Y}\right) \tag{19}$$

where $m(mX,nY)$ is the value of $m(x,y)$ given by equation (1a) at the sampling points $(mX,nY)$. The area of the corresponding resel R is XY. The Shannon-Whittaker sampling theorem states that the reconstruction $m_R(x,y)$ is equal to the signal $m(x,y)$ if $m(x,y)$ has been sufficiently sampled (i.e., $\sigma_a^2 = 0$).

It is occasionally desirable to produce spatially smoothed reconstructions, for example, to gain increased radiometric accuracy of the reconstructed signal at the cost of spatial resolution. Spatial smoothing can be accomplished by narrowing the passband of the reconstruction filter. It is convenient to express the reconstruction filter as a function of the equivalent IFOV $\gamma$ as

$$\Pi(\gamma M\upsilon, \gamma N\omega) = \begin{cases} 1 & \left(|\upsilon| < \frac{1}{2\gamma M},\ |\omega| < \frac{1}{2\gamma N}\right) \\ 0 & \text{(elsewhere)} \end{cases} \tag{20}$$

where M and N are constants. The smoothed reconstruction is

$$\bar{m}_R(x,y) = \frac{XY}{\gamma M \gamma N} \sum_{m=-\infty}^{\infty} \sum_{n=-\infty}^{\infty} m(mX,nY)\ \text{sinc}\left(\frac{x - mX}{\gamma M}\right) \text{sinc}\left(\frac{y - nY}{\gamma N}\right) \tag{21}$$

The area of the corresponding resel R is $\gamma^2 MN$. The variance of the signal and aliased noise of $\bar{m}_R(x,y)$ is given by

$$\bar{\sigma}_s^2 = \int_{-1/2\gamma M}^{1/2\gamma M} \int_{-1/2\gamma N}^{1/2\gamma N} \hat{\Phi}_s(\upsilon,\omega)\ d\upsilon\ d\omega \tag{22}$$

and

$$\bar{\sigma}_a^2 = \int_{-1/2\gamma M}^{1/2\gamma M} \int_{-1/2\gamma N}^{1/2\gamma N} \hat{\Phi}_a(\upsilon,\omega;X,Y)\ d\upsilon\ d\omega \tag{23}$$

## COMPUTATIONAL RESULTS

Figures 6 to 8 characterize the (normalized) standard deviations of the signal, aliased noise, and signal-to-noise ratio of spatially unsmoothed and smoothed reconstructions of the discrete measurements $m(x,y;X,Y)$. The standard deviations of the signal $\sigma_s$ and the aliased noise $\sigma_a$ are normalized with respect to the standard deviation $\sigma_L$ of the radiance fluctuations; the sampling intervals $X$ and $Y$ and the mean spatial width $\mu_r$ of the radiance fluctuations are normalized with respect to the equivalent IFOV $\gamma$. These normalizations permit the computational results to be applied to a wide range of practical situations.

Figure 6 presents the variation of the signal, aliased noise, and signal-to-noise ratio versus sampling intervals for various mean spatial widths of the radiance fluctuations. These results characterize the unsmoothed signal reconstructions depicted by equations (16) to (19).

Figure 7 presents these variations for the smoothed signal reconstructions formulated by equations (20) to (23). It may be noted that the conditions (and results) for $X/\gamma = Y/\gamma = 1$ and $M = N = 1$ are the same as those in figure 6 for $X/\gamma = Y/\gamma = 1$.

Figure 8 presents the same computational results as figure 7. The difference is that figure 7 shows variations in performance plotted against sampling interval while figure 8 shows variations plotted against mean spatial width of the radiance fluctuations.

## CONCLUSIONS

1. The accuracy with which sufficiently sampled components of random radiance fluctuations (or fields) can be reconstructed, as accounted for by $\sigma_s/\sigma_L$, tends to be independent of reasonable photosensor aperture shapes of equal area; however, the degradation of this accuracy by insufficiently sampled components of the radiance fluctuations, as accounted for by the aliased noise $\sigma_a/\sigma_L$, depends strongly on these aperture shapes. This conclusion is consistent with the observation by Mertz and Gray (Bell Syst. Tech. J., vol. 13, July 1934) and by Schade (J. SMPTE, vol. 64, Nov. 1955) that all reasonable photosensor aperture shapes and profiles of equivalent size result in about equal blurring, but that some shapes and profiles tend to suppress aliasing better than others.

2. Spatial smoothing (i.e., low-pass filtering) of discrete measurements decreases both the accuracy with which the sufficiently sampled radiance fluctuations (i.e., $\bar{\sigma}_s/\sigma_L$) can be reconstructed in the absence of aliased noise and the degradation of this accuracy by the presence of aliased noise (i.e., $\bar{\sigma}_a/\sigma_L$). There is a net gain in the signal-to-noise ratio $\bar{\sigma}_s/\bar{\sigma}_a$ of smoothed reconstructions because $\bar{\sigma}_a$ tends to decrease more rapidly with smoothing than $\bar{\sigma}_s$.

3. Aliased noise is a large source of error in continuous reconstructions of discrete measurements obtained with contiguous coverage, unless the mean spatial width of the (random) radiance fluctuations is more than an order of

magnitude larger than the instantaneous field of view (IFOV) of the radiometer (i.e., unless $\mu_r/\gamma > 10$). For example, for a circular IFOV and for unsmoothed reconstructions, the signal-to-noise ratio $\sigma_s/\sigma_a$ is only 16 for $\mu_r/\gamma = 9$, 5 for $\mu_r/\gamma = 1$, and 1.4 for $\mu_r/\gamma = 1/9$.

4. A decrease of about 2 orders of magnitude in aliased noise and a corresponding increase in signal-to-noise ratio are attained by modestly decreasing the sampling interval (by a factor of 0.7) and by shaping the effective IFOV (i.e., photosensor aperture and electronic filter) of a scanning radiometer. This improvement tends to be independent of the statistical properties of the radiance fluctuations. For example, the signal-to-noise ratio $\sigma_s/\sigma_a$ for unsmoothed reconstructions is increased from 16 to 514 for $\mu_r/\gamma = 9$, from 5 to 139 for $\mu_r/\gamma = 1$, and from 1.4 to 26 for $\mu_r/\gamma = 1/9$.

5. A much more modest improvement is attained at the cost of spatial resolution by smoothing (i.e., low-pass filtering) of the discrete measurements. The signal-to-noise ratio $\bar{\sigma}_s/\bar{\sigma}_a$ obtained with a circular IFOV tends to increase by about the same factor by which the reconstructed resolution is decreased. The diamond IFOV (with electronic filter) provides a more favorable trade-off.

6. For unsmoothed reconstructions, the aliased noise $\sigma_a/\sigma_L$ decreases and the signal-to-noise ratio $\sigma_s/\sigma_a$ increases with decreasing sampling interval. The rate of change varies: relatively rapid improvements can be attained by decreasing the sampling intervals $X/\gamma = Y/\gamma$ from 1 to 0.7; further decreases in sampling intervals provide less improvement. For smoothed reconstructions, the variation of $\bar{\sigma}_a/\sigma_L$ and $\bar{\sigma}_s/\bar{\sigma}_a$ with sampling intervals can exhibit intermediate dips and peaks, respectively. This occurs when the zero crossing of the neighboring sampling sidebands falls into the (narrow) low-pass reconstruction filter.

7. The standard deviations of the signal $\sigma_s/\sigma_L$ and the signal-to-noise ratio $\sigma_s/\sigma_a$ decrease monotonically as the mean spatial detail $\mu_r$ decreases, whereas the standard deviation of the aliased noise $\sigma_a/\sigma_L$ reaches a broad maximum when the mean spatial detail $\mu_r$ is slightly smaller than the IFOV $\gamma$ (i.e., when $0.1 < \mu_r/\gamma < 1$).

Langley Research Center
National Aeronautics and Space Administration
Hampton, VA 23665
March 13, 1980

## REFERENCES


1. Mertz, P.; and Gray, F.: Theory of Scanning and Its Relation to Characteristics of Transmitted Signal in Telephotography and Television. Bell Syst. Tech. J., vol. 13, no. 3, July 1934, pp. 464-515.

2. Schade, Otto H.: Image Gradation, Graininess and Sharpness in Television and Motion Picture Systems.
   Part I: Image Structure and Transfer Characteristics. J. SMPTE, vol. 56, no. 2, Feb. 1951, pp. 137-177.
   Part II: The Grain Structure of Motion Picture Images - An Analysis of Deviations and Fluctuations of the Sample Number. J. SMPTE, vol. 58, no. 3, Mar. 1952, pp. 181-222.
   Part III: The Grain Structure of Television Images. J. SMPTE, vol. 61, no. 2, Aug. 1953, pp. 97-164.
   Part IV, A & B: Image Analysis in Photographic and Television Systems (Definition and Sharpness). J. SMPTE, vol. 64, no. 11, Nov. 1955, pp. 593-617.

3. Callahan, L. G.; and Brown, W. M.: One- and Two-Dimensional Processing in Line Scanning Systems. Appl. Opt., vol. 2, no. 4, Apr. 1963, pp. 401-407.

4. Macovski, A.: Spatial and Temporal Analysis of Scanned Systems. Appl. Opt., vol. 9, no. 8, Aug. 1970, pp. 1906-1910.

5. Biberman, Lucien M., ed.: Perception of Displayed Information. Plenum Press, Inc., c.1973.

6. Katzberg, Stephen J.; Huck, Friedrich O.; and Wall, Stephen D.: Photosensor Aperture Shaping To Reduce Aliasing in Optical-Mechanical Line-Scan Imaging Systems. Appl. Opt., vol. 12, no. 5, May 1973, pp. 1054-1060.

7. Robinson, A. H.: Multidimensional Fourier Transforms and Image Processing With Finite Scanning Apertures. Appl. Opt., vol. 12, no. 10, Oct. 1973, pp. 2344-2352.

8. Pearson, D. E.: Transmission and Display of Pictorial Information. John Wiley & Sons, Inc., 1975, pp. 51-90.

9. Gonsalves, Robert A.; and Considine, Philip S.: Spot Shaping and Incoherent Optical Smoothing for Raster Scanned Imagery. Opt. Eng., vol. 15, no. 1, Jan./Feb. 1976, pp. 64-67.

10. Pratt, William K.: Digital Image Processing. John Wiley & Sons, Inc., c.1978.

11. Bracewell, Ron: The Fourier Transform and Its Applications. McGraw-Hill Book Co., c.1965.

12. Goodman, Joseph W.: Introduction to Fourier Optics. McGraw-Hill Book Co., Inc., c.1968.

13. Rosenfeld, Azriel; and Kak, Avinash C.: Digital Picture Processing. Academic Press, Inc., 1976.

14. Takagi, T.; and Tutumi, S.: Statistical Properties of Radiance Spatial Distribution of Sky and Forest Backgrounds. Electron. & Commun. Japan, vol. 51, no. 2, Feb. 1968, pp. 82-90.

15. Itakura, Yasumasa; Tsutsumi, Suteo; and Takagi, Tehru: Statistical Properties of the Background Noise for the Atmospheric Windows in the Intermediate Infrared Region. Infrared Phys., vol. 14, no. 1, Feb. 1974, pp. 17-29.

16. Lee, Y. W.: Statistical Theory of Communication. John Wiley & Sons, Inc., c.1960.

17. Blackman, R. B.; and Tukey, J. W.: The Measurement of Power Spectra. Dover Publ., Inc., 1959.

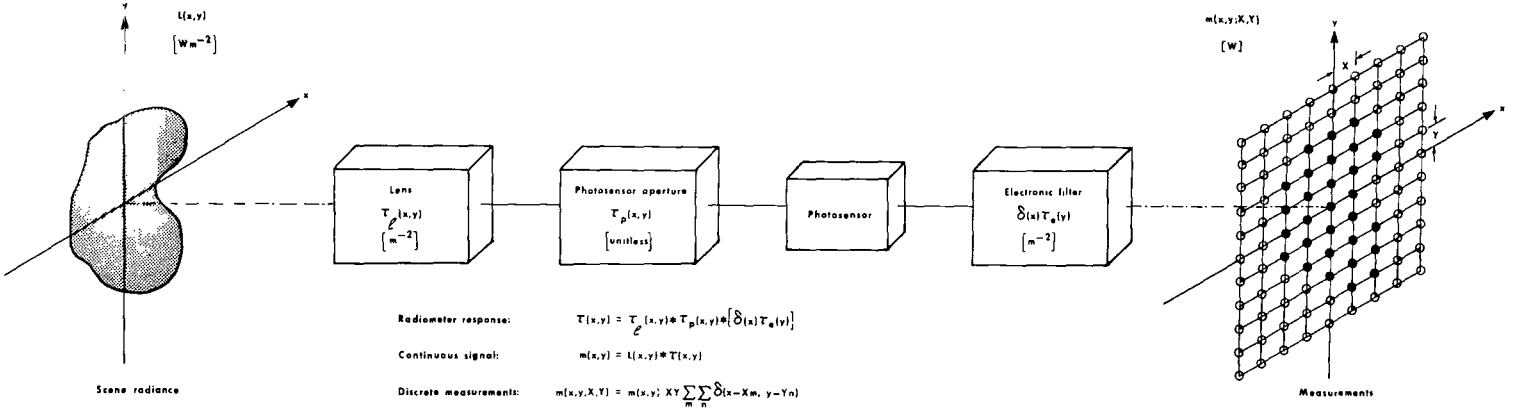


Figure 1.- Measurement process.

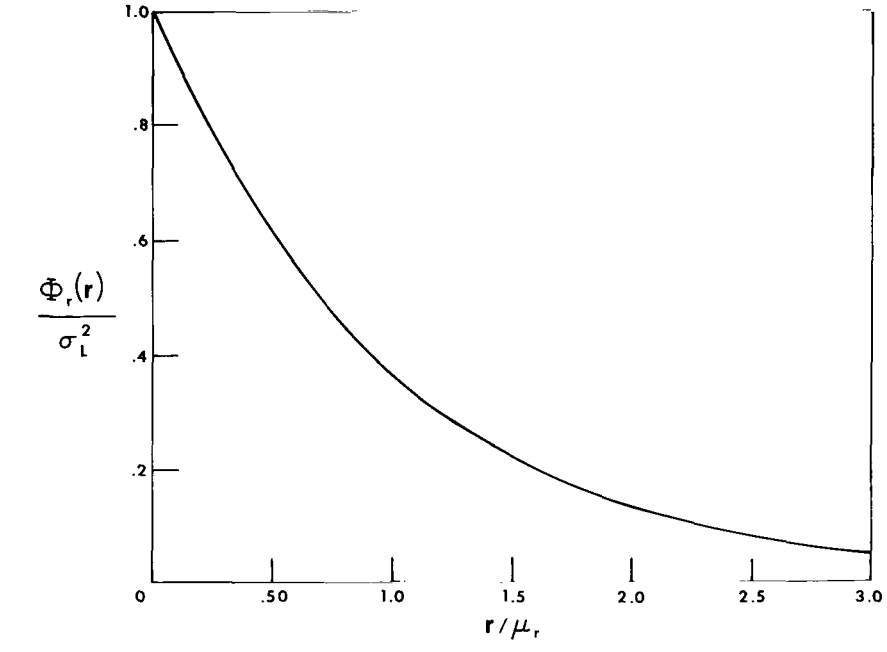


(a) Autocovariance.

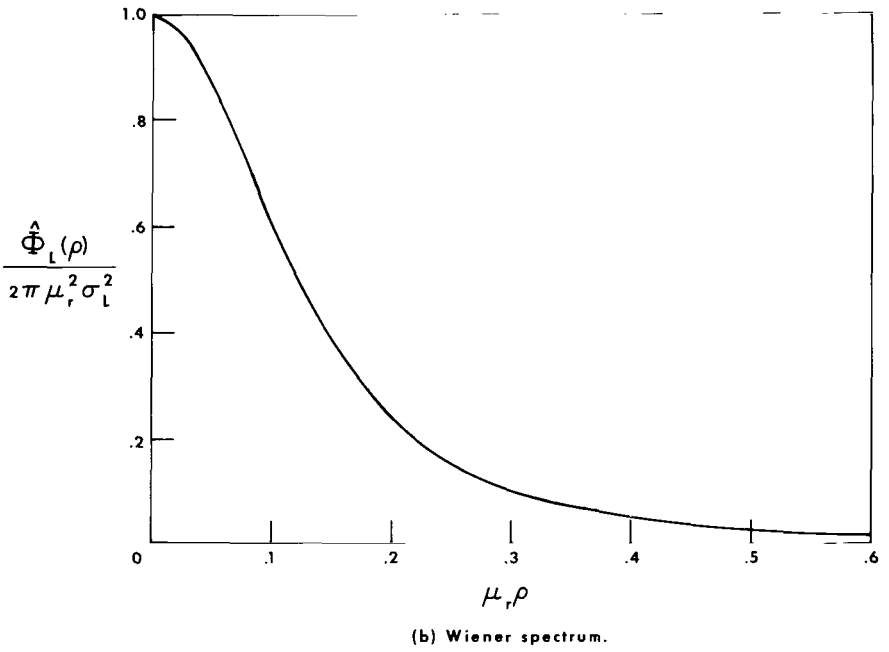


(b) Wiener spectrum.

Figure 2.- Properties of radiance fluctuations.

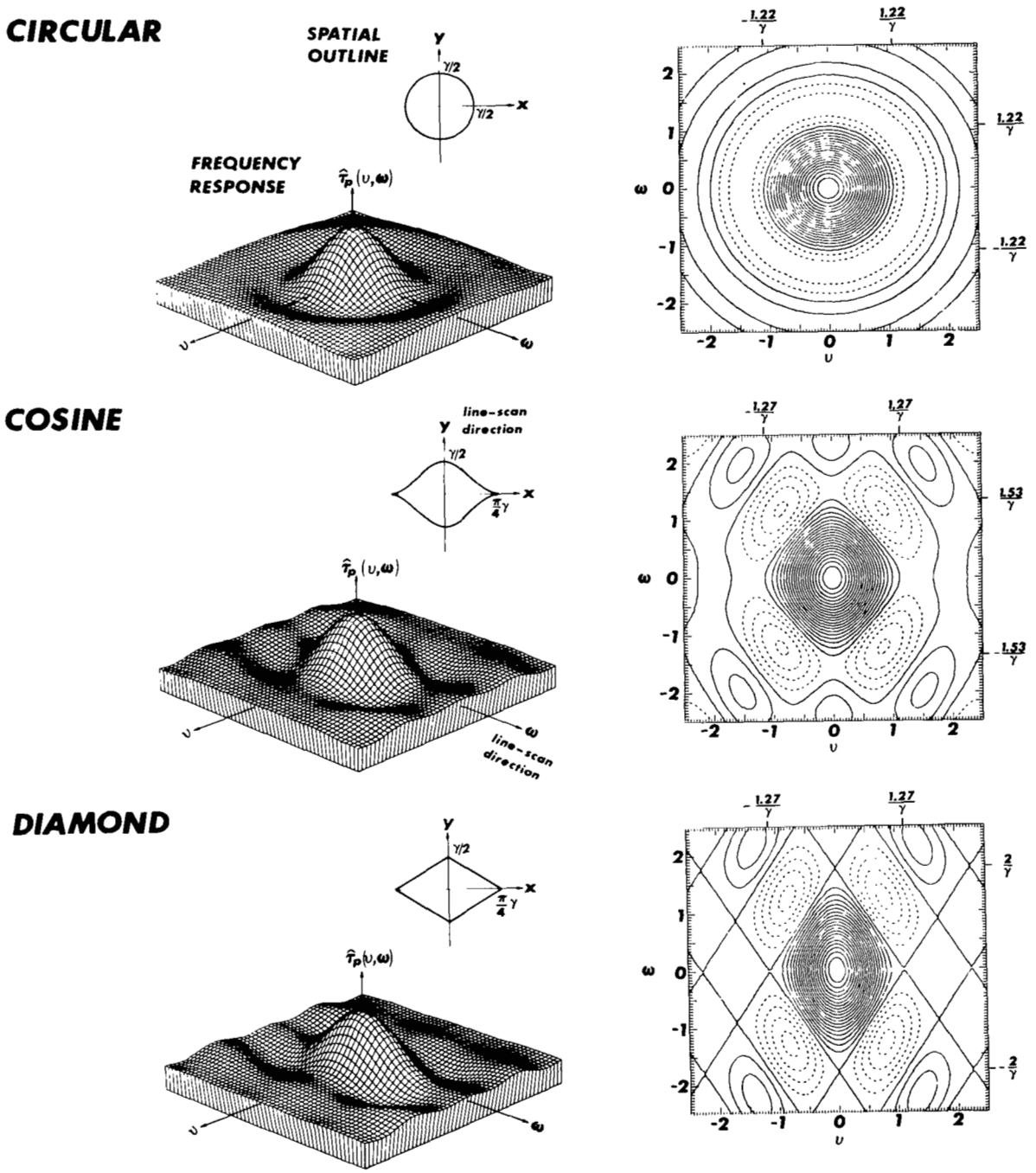


Figure 3.- Spatial outline and frequency response of photosensor apertures with equal area. Parameter $\gamma$ is defined as effective IFOV formed by apertures; contour plots are labeled for $\gamma = \sqrt{4/\pi} = 1.13$. Cosine and diamond IFOV's are continuously scanned along y-direction so that resulting analog signal can be electronically filtered. (Solid and broken lines in contour plot represent positive and negative values, respectively.)

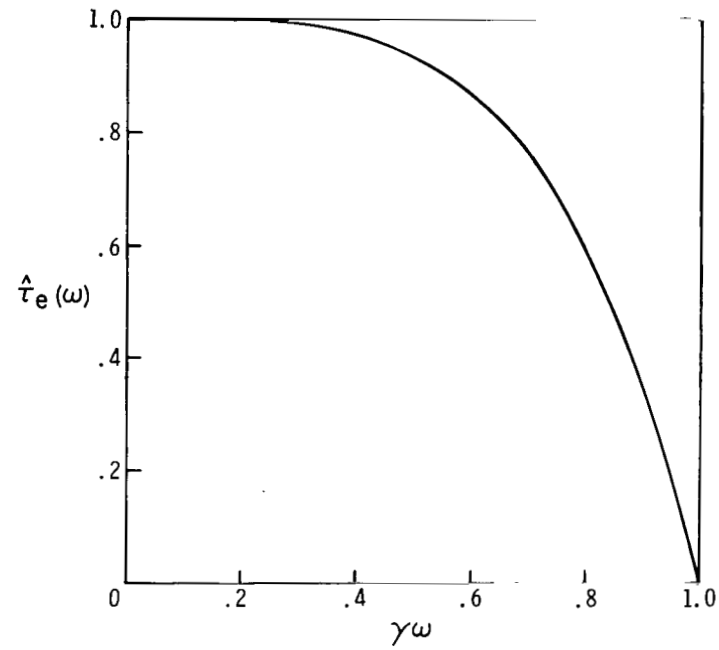


**Figure 4.- Spatial frequency response of electronic filter.**

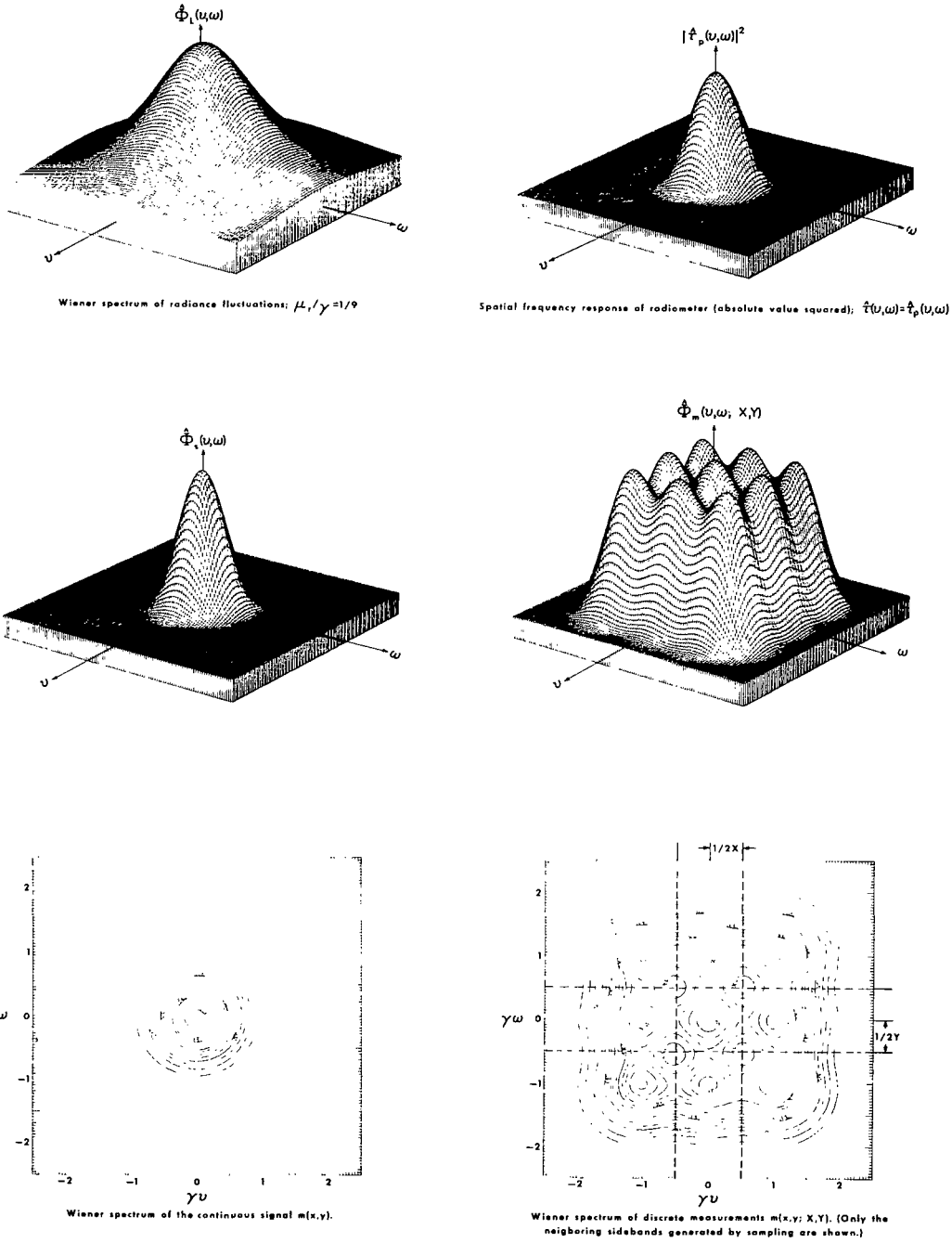


(a) Common measurement process: contiguous coverage (i.e., $X/\gamma = Y/\gamma = 1$) with discretely stepped, circular IFOV.

Figure 5.- Measurement characteristics in spatial frequency domain. Only neighboring sampling sidebands shown here have been included in computation of aliased noise; more accurate computations that include additional sidebands would yield slightly larger magnitudes of aliased noise.

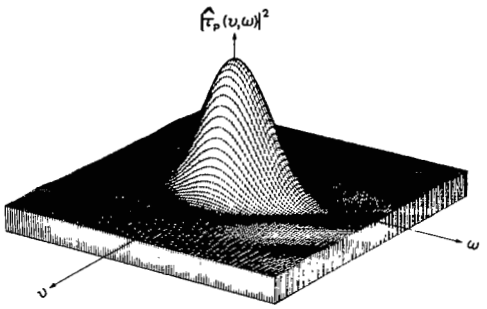


Spatial frequency response of photosensor aperture (absolute value squared)

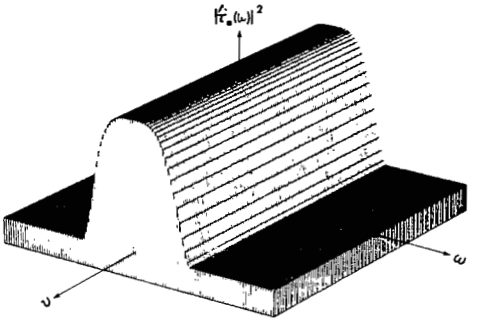


Spatial frequency response of electronic filter (absolute value squared).

Spatial frequency response of radiometer (absolute value squared): $|\hat{\tau}(\upsilon,\omega)|^2 = |\hat{\tau}_p(\upsilon,\omega)|^2 |\hat{\tau}_e(\omega)|^2$

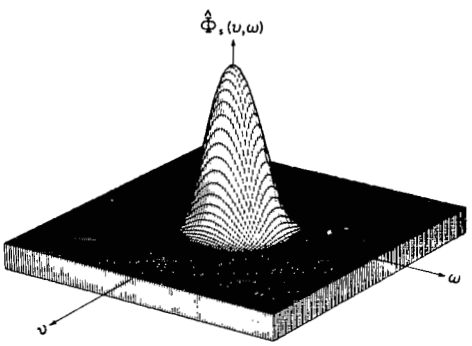


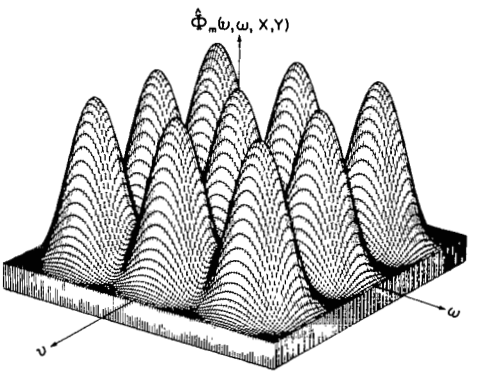


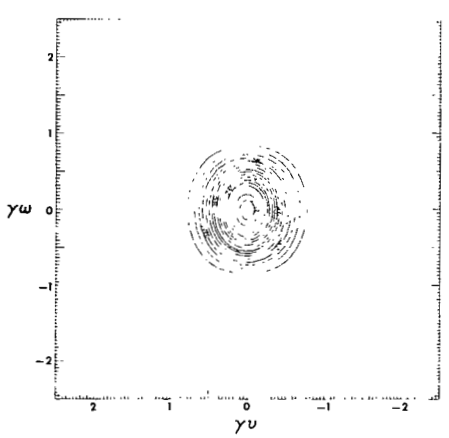


Wiener spectrum of the continuous signal m(x,y)

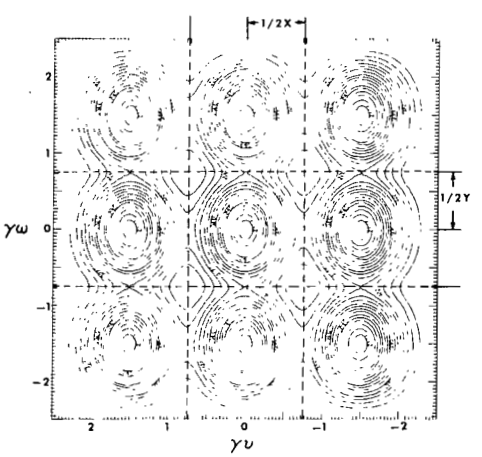


Wiener spectrum of discrete measurements m(x,y; X,Y). (Only the neighboring sidebands generated by sampling are shown.)

(b) Improved measurement process: overlapping coverage (i.e., X/γ = Y/γ 0.7) with continuously scanned, diamond IFOV and electronic filter.

Figure 5.- Concluded.

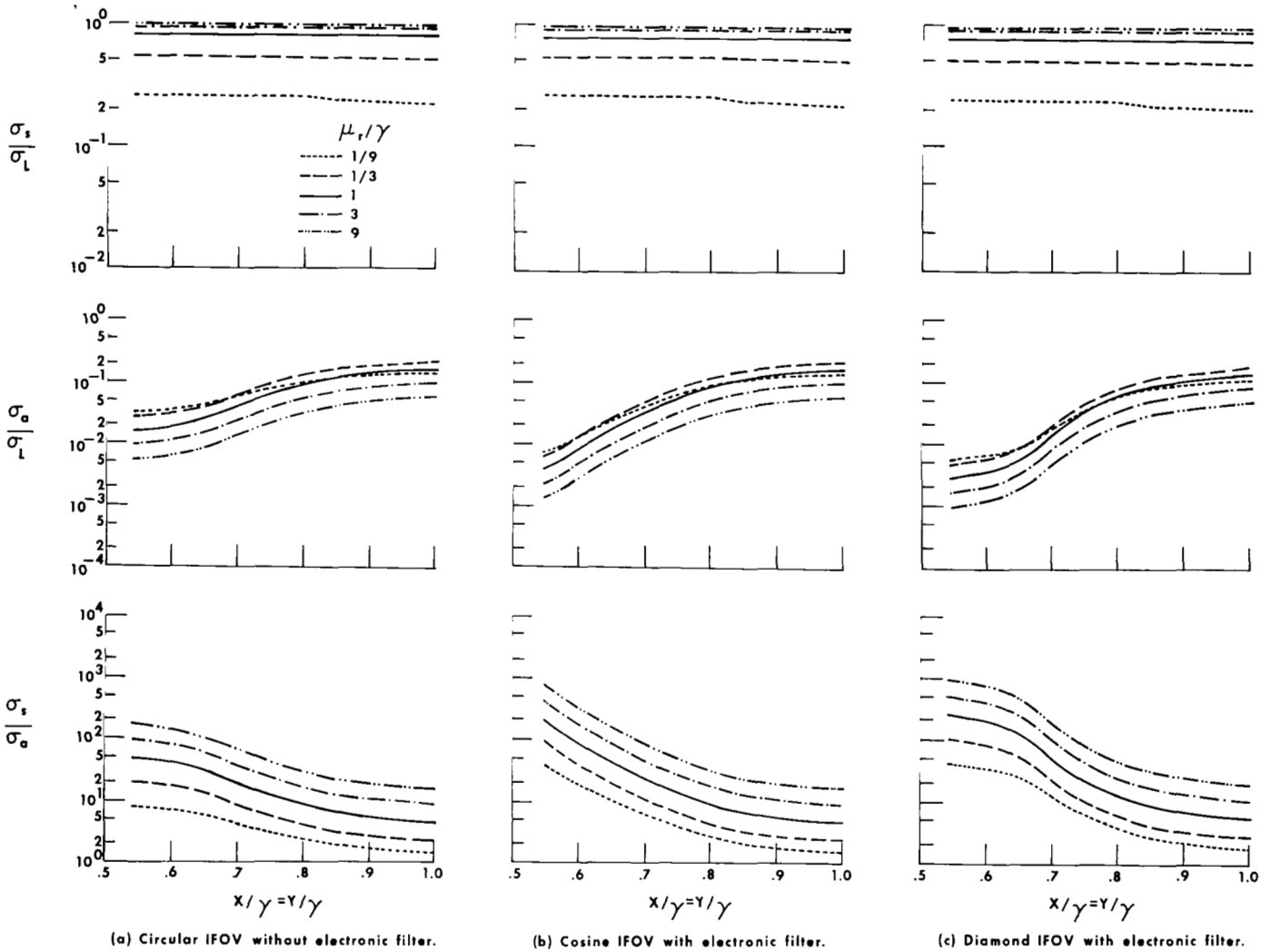


Figure 6.- Variation of standard deviation of normalized signal $\sigma_s/\sigma_L$, aliased noise $\sigma_a/\sigma_L$, and of signal-to-noise ratio $\sigma_s/\sigma_a$, versus sampling intervals $X/\gamma = Y/\gamma$ for various mean spatial detail widths $\mu_r/\gamma$ of radiance fluctuations $L(x,y)$. These results characterize unsmoothed reconstructions formulated by equations (16) to (19). Area of resel R is XY.

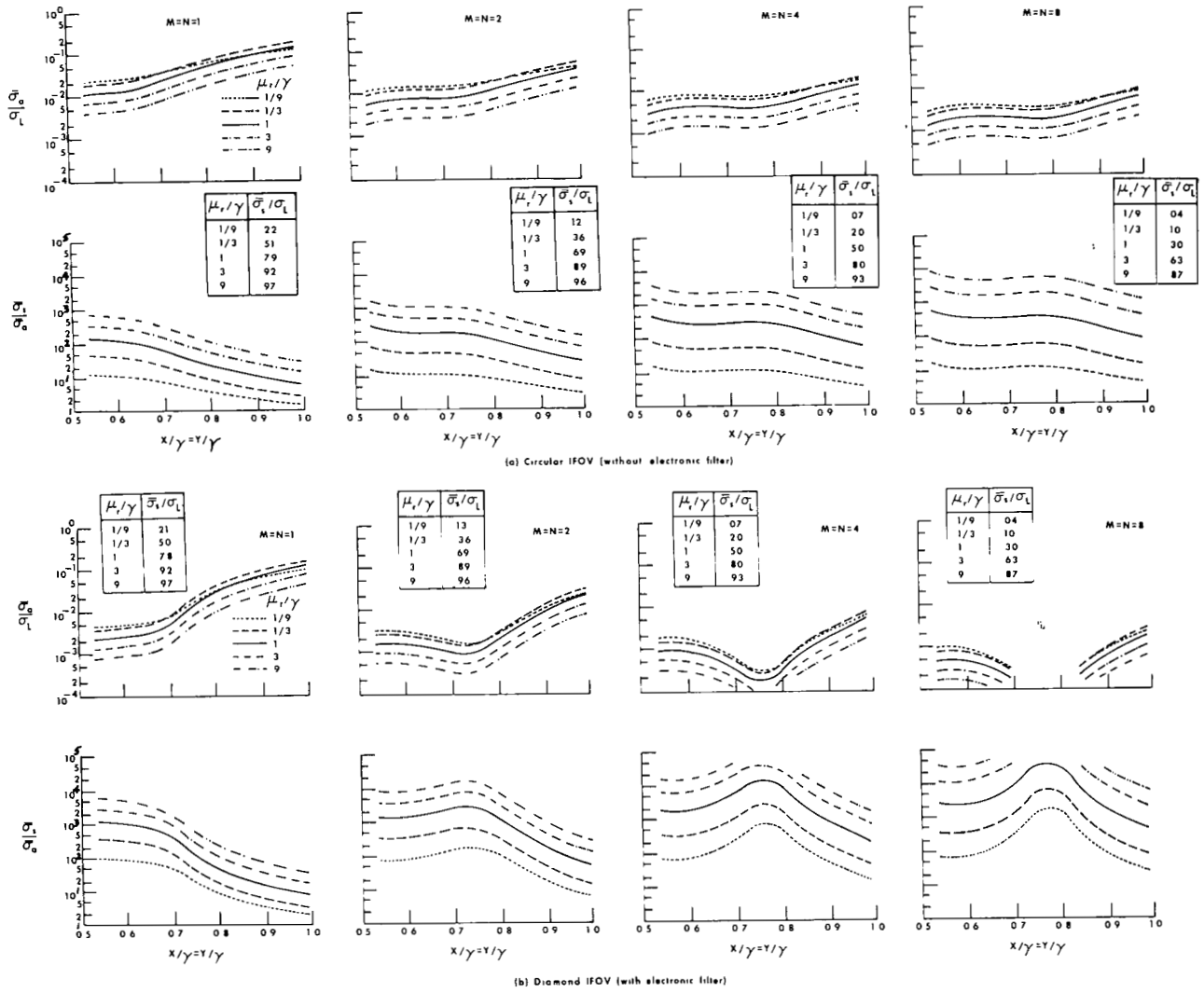


Figure 7.- Variation of standard deviation of normalized aliased noise $\bar{\sigma}_a/\sigma_L$, and of signal-to-noise ratio $\bar{\sigma}_s/\bar{\sigma}_a$ versus sampling intervals $X/\gamma = Y/\gamma$ for various mean spatial detail widths $\mu_r/\gamma$ of radiance fluctuations $L(x,y)$. These results characterize smoothed reconstruction formulated by equations (20) to (23). Area of resel R is $\gamma^2MN$; number of measurements encompassed by R is $\gamma^2MN/XY$ (e.g., MN if $X/\gamma = Y/\gamma = 1$, and 4MN if $X/\gamma = Y/\gamma = 0.5$).

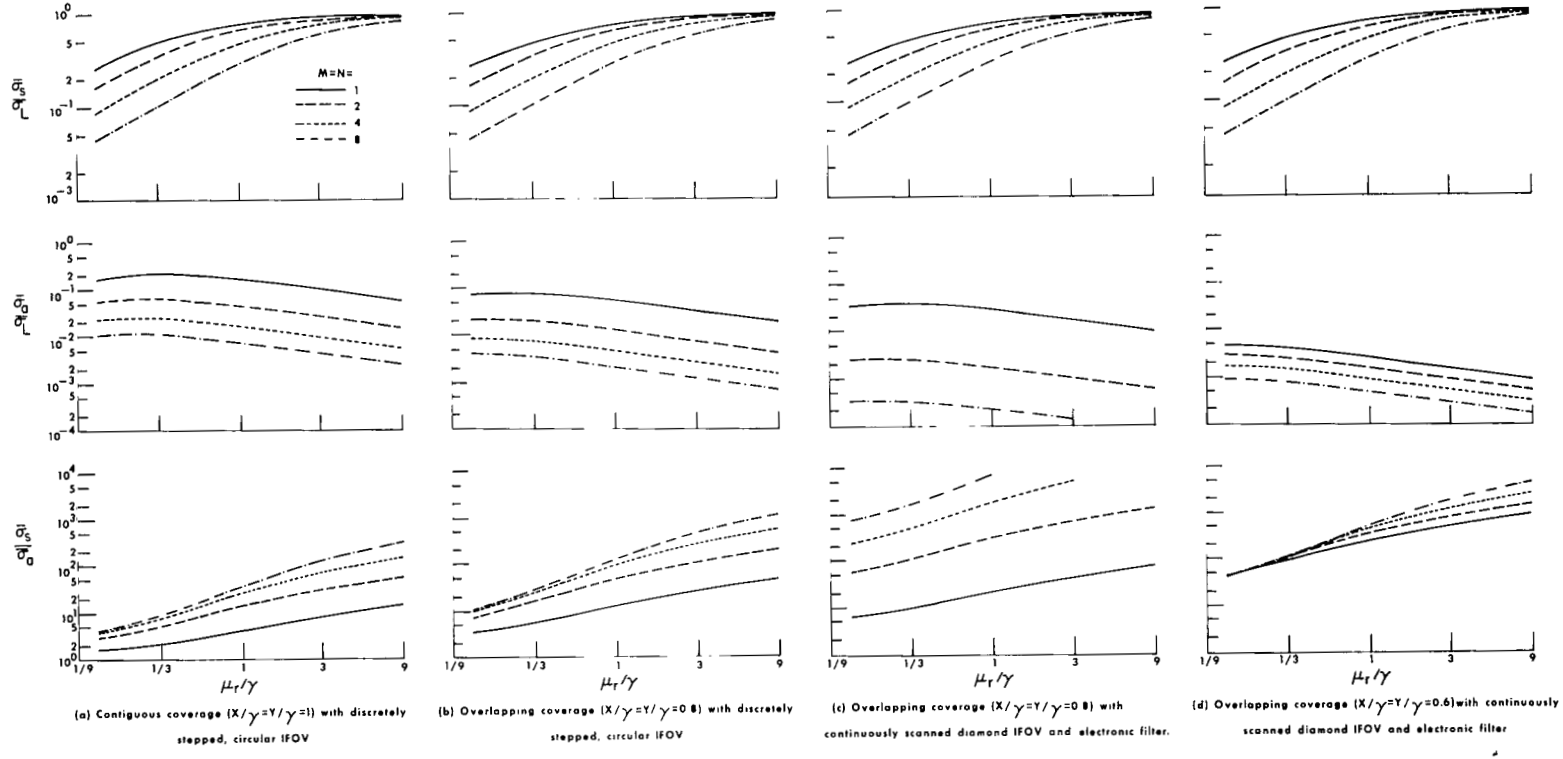


Figure 8.- Variation of standard deviation of normalized signal $\bar{\sigma}_s/\sigma_L$ and aliased noise $\bar{\sigma}_a/\sigma_L$, and of signal-to-noise ratio $\bar{\sigma}_s/\bar{\sigma}_a$ versus mean spatial detail widths $\mu_r/\gamma$. These results characterize smoothed reconstructions formulated by equations (20) to (23).

| 1. Report No. | 2. Government Accession No. | 3. Recipient's Catalog No. |
|---|---|---|
| NASA TP-1639 | | |

| 4. Title and Subtitle | 5. Report Date |
|---|---|
| ALIASED NOISE IN RADIOMETRIC MEASUREMENTS | May 1980 |
| | 6. Performing Organization Code |

| 7. Author(s) | 8. Performing Organization Report No. |
|---|---|
| Friedrich O. Huck, Stephen K. Park, Nesim Halyo, and Steven T. Stallman | L-13410 |
| | 10. Work Unit No. 619-12-01-01 |

| 9. Performing Organization Name and Address | 11. Contract or Grant No. |
|---|---|
| NASA Langley Research Center<br>Hampton, VA 23665 | |
| | 13. Type of Report and Period Covered<br>Technical Paper |

| 12. Sponsoring Agency Name and Address | 14. Sponsoring Agency Code |
|---|---|
| National Aeronautics and Space Administration<br>Washington, DC 20546 | |

15. Supplementary Notes

Friedrich O. Huck and Stephen K. Park: Langley Research Center.
Nesim Halyo and Steven T. Stallman: Information and Control Systems, Hampton, Va.

16. Abstract

The reconstructed magnitude of radiance fluctuations (or fields) from discrete radiometric measurements is subject to errors caused by the aliased noise generated when the radiometer undersamples the spatial detail of these fluctuations. Quantitative results indicate that aliased noise can be a large source of error in the reconstruction process when the sampling intervals equal the instantaneous field of view (IFOV) of the radiometer (i.e., for contiguous coverage). This noise can be reduced about 2 orders of magnitude by shaping the effective IFOV (formed by the photosensor aperture and signal electronics) of a scanning radiometer and modestly decreasing the sampling intervals relative to the IFOV (to provide some overlap between successive measurements). In contrast, spatially smoothed (i.e., low-pass filtered) reconstructions of the discrete measurements provide only a relatively modest decrease in this noise at the cost of spatial resolution.

| 17. Key Words (Suggested by Author(s)) | 18. Distribution Statement |
|---|---|
| Aliased noise<br>Optical-mechanical scanner<br>Radiometric measurements | Unclassified - Unlimited<br><br>Subject Category 35 |

| 19. Security Classif. (of this report) | 20. Security Classif. (of this page) | 21. No. of Pages | 22. Price* |
|---|---|---|---|
| Unclassified | Unclassified | 23 | $4.00 |

* For sale by the National Technical Information Service, Springfield, Virginia 22161

NASA-Langley, 1980

3 1 1U,D, 042180 S00903DS
DEPT OF THE AIR FORCE
AF WEAPONS LABORATORY
ATTN: TECHNICAL LIBRARY (SUL)
KIRTLAND AFB NM 87117